Temperature Sensitivity Control of an Inkjet-Printed Optical Resonator on Pillar

Marc-Antoine Bianki,* Régis Guertin, Cédric Lemieux-Leduc, and Yves-Alain Peter

Department of Engineering Physics, Polytechnique Montréal, Montréal, QC, H3T 1J4, Canada

E-mail: marc-antoine.bianki@polymtl.ca

Abstract

We report a whispering gallery mode resonator on pillar using inkjet printing combined with traditional microfabrication techniques. This approach enables several different polymers on the same chip for sensing applications. However, polymers inherently exhibit sensitivity to multiple stimuli. To mitigate the temperature sensitivity, careful selection of design parameters is crucial. By precisely tuning the undercut-to-radius ratio of the resonator, a linear dependance in temperature sensitivity ranging from $-41.5\,\mathrm{pm/°C}$ to $23.4\,\mathrm{pm/°C}$, with a zero-crossing point at $47.6\,\%$ is achieved. Consequently, it is feasible to fabricate sensing devices based on undercut microdroplets with minimal temperature sensitivity. The lowest measured temperature sensitivity obtained was $5.9\,\mathrm{pm/°C}$, for a resonator with an undercut-to-radius ratio of $53\,\%$.

Keywords

Whispering gallery modes, Optical sensors, Microcavities, Temperature sensors, Thermal expansion, Thermo-optic effects, Inkjet printing, Microfabrication

1 Introduction

Polymers, as stimuli-responsive materials, are widely studied for sensing various parameters[1]. Among these, gas concentration measurement, crucial in food industry, air quality, mining, and healthcare[2], could benefit from their cost-effective nature and reversible behavior. These sensors can be either electronic[3,4] or optical[5].

Optical resonators exhibit exceptional suitability for polymer sensors due to their high sensitivity to small changes. They exist in diverse cavity configurations, including Fabry-Perot, microrings, microdisks, and microbottles[6]. The latter is known as whispering gallery mode resonators for which light undergoes total internal reflection at the circular boundary, resulting in high-quality factors and low mode volumes. PDMS microbottle[7] and in-fiber polymer microdisk[8] were used for sensing.

In our prior work, we investigated the gas concentration sensitivity of SU-8 disks on silicon pillars[9]. This configuration allows a section of the polymer to freely swell due to its hanging part, resulting in a tenfold increase in sensitivity to gas concentrations compared to Fabry-Perot resonators functionalized with the same polymer. However, two challenges persisted. The first challenge involves the lack of selectivity towards a single gas, as this particular polymer demonstrates sensitivity to at least six gases. The second challenge relates to temperature sensitivity, since to obtain the reported limits of detection, temperature fluctuations must be maintained below 80 mK.

Since it was shown that the affinity of polymers are different for each gas, with the response of multiple polymers, it is possible to get the concentration of each gas from a mixture[10]. However, the current microfabrication process—comprising spin coating and photolithography—restricts the utilization of only one photosensitive polymer per microchip. Additive methods like drop-on-demand inkjet printing are well suited to deposit these different polymers on the same optical microchip.

Polymeric resonators were reported to be successfully fabricated using inkjet printing and investigated for low-threshold lasing[11] and biosensing[12]. This technique proves to be

cost-effective, minimizes material wast, and enables the production of smooth surfaces with ease. This versatile technique allows for the printing of various materials, including different polymers[13–15]. Moreover, printing of multiple materials in close proximity is possible, which is advantageous to create a sensor matrix[16].

The second issue is related to the versatility of polymers since they are sensitive to other quantities than gas concentration[17]. They can be used, for example, as a temperature sensor[18] or a pH sensor[19]. This versatility is both an advantage and a disadvantage since it can lead to cross-sensitivity issues, resulting in erroneous readings of the measured values. In the case of temperature sensitivity, specifically, the high thermal expansion and thermo-optic coefficients of polymers which make them advantageous for optical temperature sensing applications[18], pose challenges when measuring other quantities[20,21].

First, temperature can be decoupled by measuring it[10,22–24]. By subtracting the contribution of the temperature, it becomes possible to extract the desired value accurately. However, since each measurement carries inherent errors, the device precision is decreased. Thus, it is still important to lower the sensitivity of the interfering quantity to some sensing elements.

Thus, another strategy would be treating the polymer matrix using high-temperature annealing[25] or incorporating materials with negative temperature coefficients[26] to mitigate the temperature sensitivity. However, it increases the material complexity. We propose an additional strategy to mitigate temperature cross-sensitivity by optimizing design parameters. Our objective revolves around minimizing sensitivity to temperature by modifying the resonator's undercut.

To address both these issues, we studied the temperature sensitivity of a polymer microdroplet on a pillar combining inkjet printing technology and microfabrication. Our main motivation is to mitigate the temperature crosstalk of inkjet-printed SU-8 resonator towards the development of a general multi-polymer sensing platform, targeting first gas sensing.

The temperature sensitivity mechanism is based on the change of the resonance condition

of the microdroplet (Fig. 1a). A rise in temperature induces polymer expansion and alters the refractive index (Fig. 1b). These phenomena are denoted as thermal expansion and thermo-optic effect, respectively. These changes lead to a shift in the resonance wavelength.

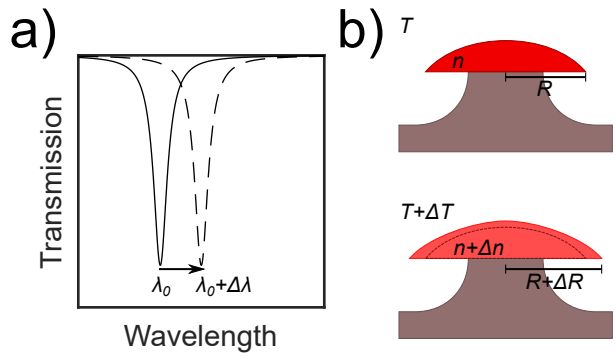

Figure 1: Temperature sensing mechanism of an all-polymer microdroplet on pillar. a) A peak shift ($\Delta\lambda$) is observed when the resonance condition varies with temperature (ΔT). b) This shift is attributed to thermal expansion (ΔR) and change of the refractive index (Δn).

SU-8 was selected for this study to follow our previous work with humidity sensitivity of SU-8 disks on a silicon pillar using photolithography[9]. Moreover, previous research has shown successful inkjet printing of this polymer[27–30] and it has been employed in the fabrication of humidity sensors[31].

2 Microfabrication and Optical Characterization

The fabrication process (Fig. 2a) begins with a cleaned silicon wafer (100 mm, <100>, p-type, 1-20 Ω cm). The substrate is dehydrated, then primed with hexamethyldisilazane (HMDS) to enhance adhesion of polymers. Drop-on-demand inkjet printing is employed to deposit SU-8 droplets (Step 1) by using MicroChem's SU-8 2000.5 (14.3 % solid in cyclopentanone) as the ink. The solution possesses a viscosity of 2.49 cP and a density of 1.070 g/mL. Printing is carried out using an inkjet printer (Microdrop Technologies) equipped with a piezoelectric-driven printing head. The printing parameters, as specified in Table 1, were optimized to ensure optimal stability during the deposition of the viscoelastic polymer ink[32]. In-

flight droplets with a radius of 60 µm are obtained (Fig. 2b). Subsequently, a softbake was conducted on a hotplate for 5 min at 95 °C (Step 2). The droplets are then exposed to UV light with a dose of 160 mJ cm^{-2} using a Karl Suss MA-6 followed by a post-exposure bake on a hotplate for 5 min at 95 °C (Step 3). To form the pillar and to release the droplet, the silicon substrate is etched with an SF_6 plasma (Step 4). An inductively coupled plasma (ICP) system (Oxford Instruments PlasmaLab ICP System 100) is used with 500 W of power employing ions acceleration, and operating at 25 mTorr. The etching time is adjusted to control the desired undercut length.

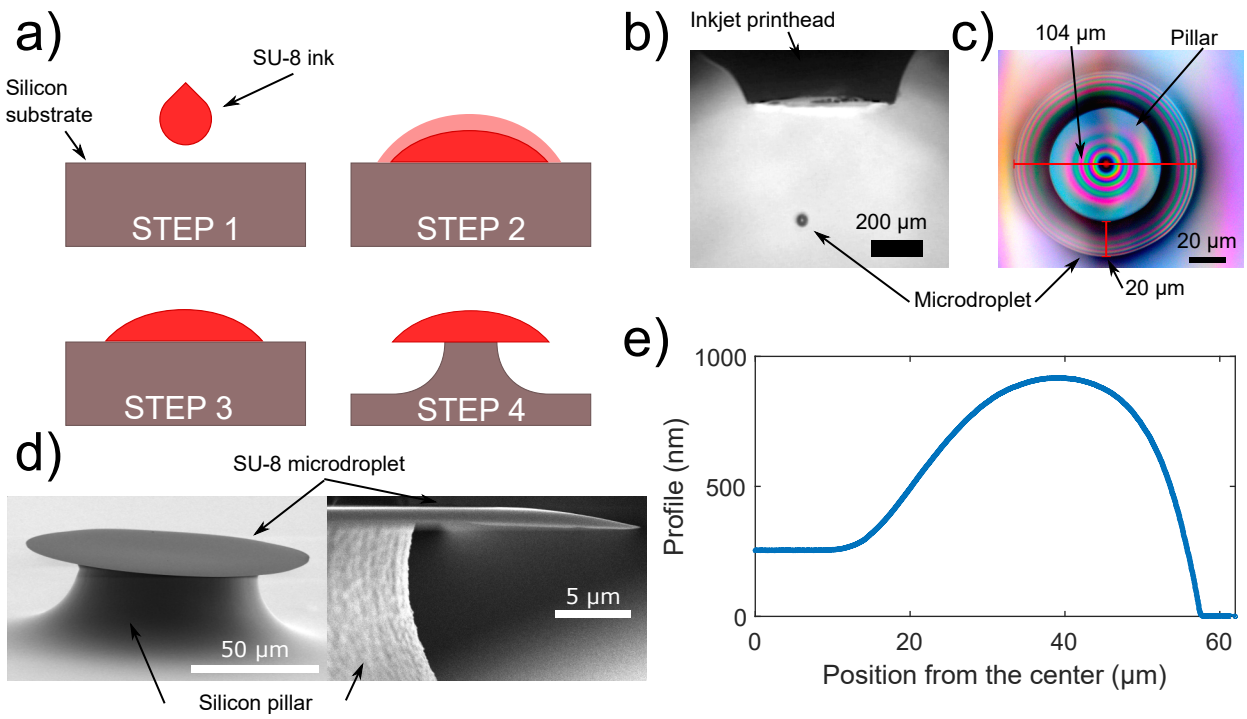

Figure 2: a) Fabrication process of a polymer microdroplet on pillar. b) In-flight inkjet-printed droplets ejected from the printhead. c) Top-down view of a microdroplet, revealing the underlying pillar. d) Scanning electron microscope images of the microdroplet on pillar. e) Radial height profile of the microdroplet.

Figure 2c shows a top view optical microscope image capturing an SU-8 microdroplet on pillar with a diameter of 104 µm and an undercut of 20 µm. Scanning electron microscopy (SEM) images (Fig. 2d) validate these values, providing both an overall and side view. The microdroplet's edge appears wedged. The profile of the droplet is further analyzed using

Table 1: Inkjet printing parameters

Parameter	Value
Voltage (V)	85
Pulse duration (µs)	25
Nozzle diameter (µm)	100
Back pressure (mbar)	−16
Nozzle temperature (°C)	25
Substrate temperature (°C)	30

profilometry, as depicted in Fig. 2e. The measurement begins at the center of the droplet and extends radially towards the edge, allowing for a comprehensive examination of its shape and dimensions. The resulting shape reveals a central plateau with a thickness of 254 nm. Additionally, a specific area positioned at a distance of 39.2 µm from the center exhibits a significantly higher thickness of 918 nm. This profile indicates the presence of the coffee ring effect,[33] influenced by the rate of solvent evaporation and controllable with the substrate temperature.The surface morphology play also a role in the profile shape. The smooth, hydrophobic and homogeneous surface prior to the deposition ensures the circular symmetric structure essential for a whispering gallery mode resonator. Finally, the radial profile will impact slightly both the effective radius and the refractive index of the resonance optical mode where the edge wedge will push the mode inward[34]. This only affects temperature or gas concentration sensitivity minimally. Nevertheless, for consistency in the process, the substrate temperature was maintained at 30 °C.

Optical characterization was performed by taking the transmission spectrum of a tapered optical fiber (SMF-28e) with a diameter of about 1 µm coupled to the microdroplet. The optical fiber was positioned on the top surface and at the edge of the microdroplet using multi-axis precision stages. A tunable laser source is synchronized with an optical power meter to acquire the transmission spectrum. Resonances of both transverse electric (TE) and transverse magnetic (TM) modes were observed. To optimize the optical fiber mode to align with either of these resonant modes, a polarization controller was used.

Figure 3 shows an example of a transmission spectrum spanning over four free spectral ranges (FSR) which is 5 nm with six distinct modes represented by six minima. A closer examination around 1543.64 nm allows the measurement of the full width at half-maximum (FWHM) of the peak, which amounts to 106.1 pm. This measurement allows for the determination of the quality factor (Q-factor), yielding a value of 1.46×10^4. This value surpasses that of the photolithography SU-8 resonator[31] which has a Q-factor of 10^3. The surface tension of the droplet helps in smoothing the SU-8/air interface and decreases surface scattering loss. Moreover, it outperforms previous inkjeted microcavities[35] exhibiting a Q-factor of 10^4.

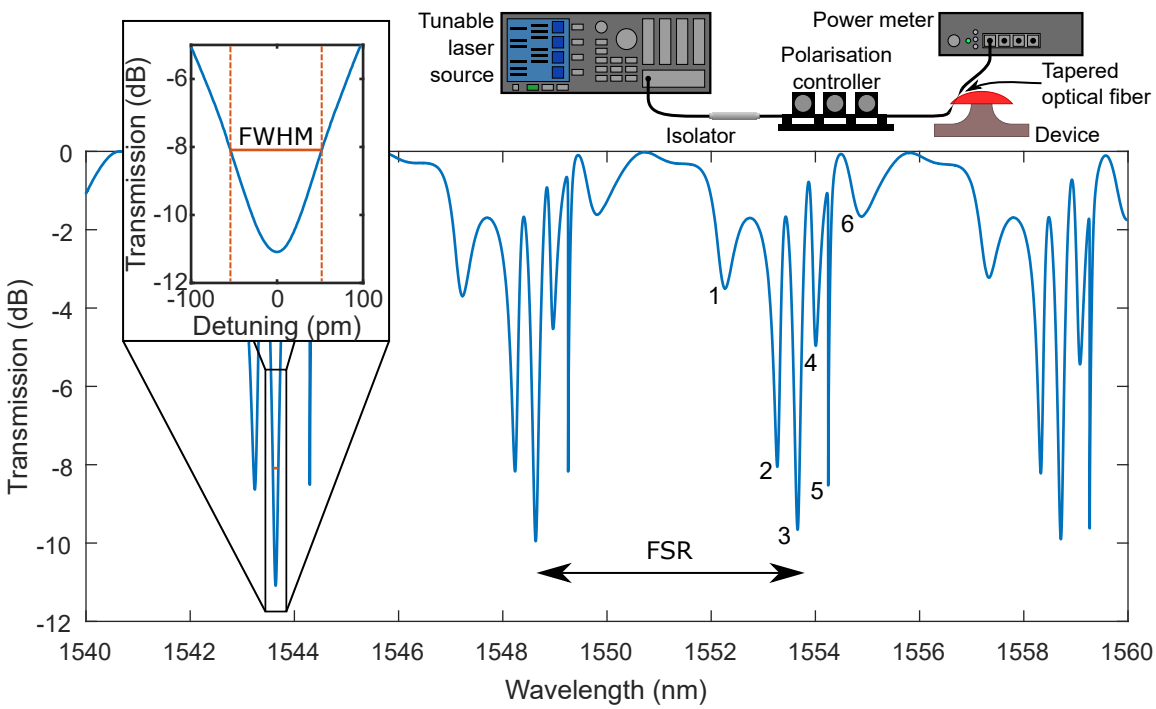

Figure 3: Optical transmission spectrum of a tapered optical fiber coupled to a microdroplet on pillar with a close-up view of a peak, along with a schematic representation of the experimental setup utilized.

3 Temperature Sensitivity Measurements

In order to assess the temperature sensitivity of the device, it is packaged within a compact enclosure and exposed to a controlled nitrogen flow with a flow rate of 5000 sccm regulated

by a mass flow controller depicted in Fig. 4a. The temperature is controlled through a dual approach. Firstly, the chip is positioned on a thermoelectric module that is interfaced with a PID controller (MTD1020T). Secondly, the nitrogen flow passes troughs a heated copper block. The temperature of the nitrogen flow is measured immediately prior to its entry into the sample box. Both the temperature of the chip and the temperature of the nitrogen flow are adjusted in tandem, utilizing the same setpoint for precise temperature control.

The temperature range explored during the experiment spans from 30 °C to 44 °C which is significantly lower than the glass transition temperature of SU-8 of 210 °C. Two ramps are conducted where the initial ramp serves to condition the sensor. Transmission spectra are captured at intervals of 10 seconds. The position of each peak is recorded, as depicted in Fig. 4b. We observe a negative proportional response of the sensor as illustrated in Fig. 4c. The displacement of this peak amounts to approximately 0.6 nm for a temperature variation of 14 °C.

In order to quantify the temperature sensitivity, we conducted measurements by tracking the resonance peaks while systematically adjusting the temperature. Optical transmission spectra were acquired using the same setup employed for the initial optical characterization. At the end of each temperature plateau, the positions of the peaks were averaged over a duration of 90 seconds. By performing a linear regression analysis, the temperature sensitivity of the device was determined (Fig.4d). The control uncertainties, expressed as $3-\sigma$ errors, were found to be 7.6 m°C and 37.5 m°C for the chip and flow temperature measurements, respectively. Regarding the peak positions, the overall error was 8 pm.

These measurements were conducted on six different samples, each possessing a distinct undercut-to-radius ratio ranging from 22.5 % to 59.0 %. The corresponding sensitivities are presented in Table 2 along with the regression errors on the slope and the coefficients of determination R^2. The latter is minimal for the sample with the slightest sensitivity which gives peak displacement values near the noise level.

Table 2: Sensitivity measurements for six samples with different undercut-to-radius ratio

Ratio %	Undercut µm	Radius µm	Sensitivity pm/°C	Error pm/°C	R^2
22.5	12.8	57.1	−38.0	0.3	0.99
24.0	12.6	52.7	−41.5	0.4	0.99
32.6	17.0	52.2	−24.8	1.5	0.90
38.9	20.2	52.0	−18.3	0.6	0.84
53.3	27.4	51.4	5.9	0.6	0.62
59.1	30.9	52.3	23.4	1.6	0.92

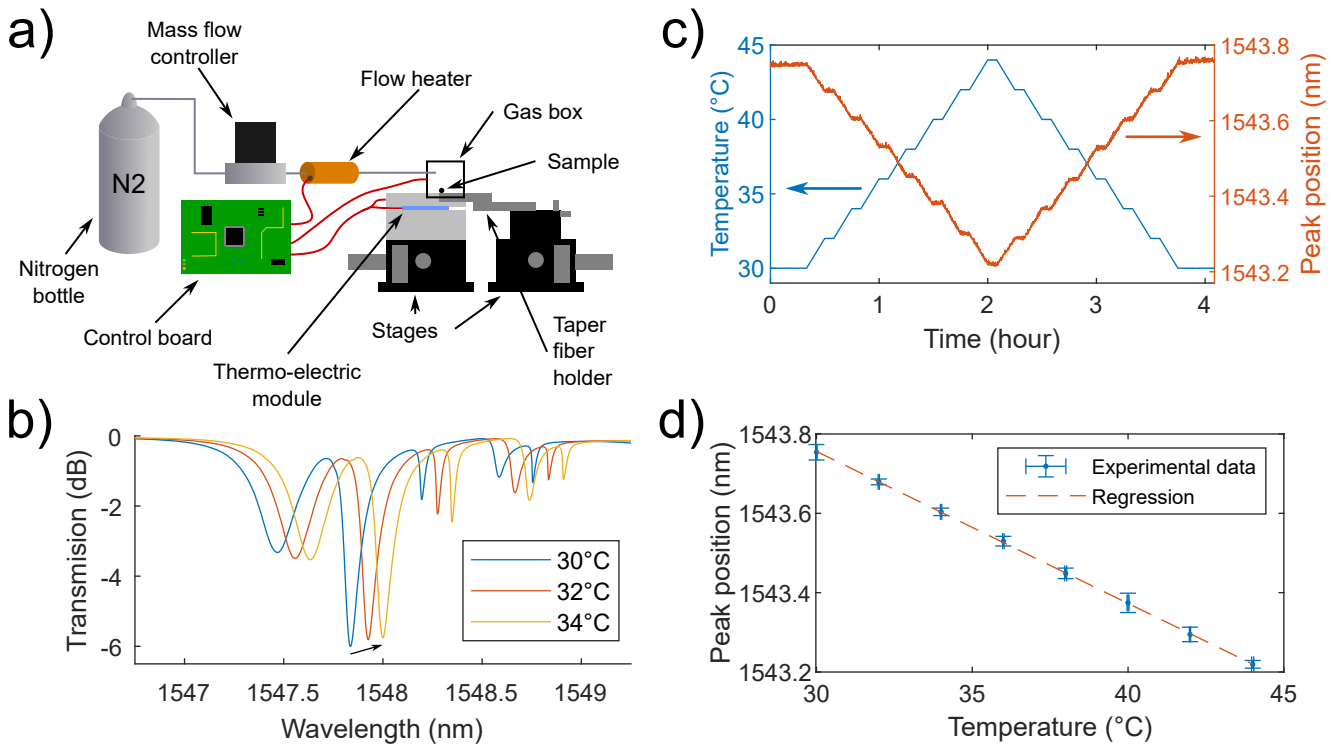

Figure 4: a) Experimental setup for the temperature sensitivity measurements. b) Spectra at different temperatures showing the peak displacement. c) Tracking of a single peak position while varying the temperature over time. d) Linear regression of the peak displacement versus temperature.

4 Modeling and Discussion

The temperature sensitivity was modeled by taking into account both the thermal expansion of the SU-8 material and its variation in refractive index with temperature, which is determined by the thermo-optic coefficient. Simulations were performed on the COMSOL software employing finite element analysis over a 2.5D axis-symmetric model of the resonator on pillar. This modeling approach takes into account the inherent cylindrical symmetry of the problem, utilizing the radial coordinate r and the axial coordinate z. The origin of the coordinate system is positioned at the center of the droplet's base. The shape of the polymer resonator was obtained by extracting the measured profile (Fig. 2e). Mechanical properties utilized in the simulations were sourced from the photoresist datasheet, with values of 60 MPa for tensile strength and 2.0 GPa for Young's modulus.

The thermal expansion and thermo-optic coefficients were determined through ellipsometry measurements. The SU-8 was spin-coated on a silicon substrate, following the same treatment as the SU-8 microdroplets in terms of UV exposure and baking. Ellipsometry measurements were performed under a nitrogen atmosphere while varying the temperature from 25 °C to 90 °C. By analyzing the changes in refractive index and thickness with temperature, the thermal expansion coefficient and the thermo-optic coefficient were calculated. The obtained coefficient of thermal expansion was 150 ppm/K, which is three times higher than the value stated in the datasheet[36] (52 ppm/K). The thermo-optic coefficient was found to be −90 ppm/K, which is half of the values reported in the literature[37–39] at −180 ppm/K. To illustrate the effects of thermal expansion, the deformation of the material was simulated for a specific temperature change of 10 °C (Fig. 5a). In a second step, and using the thermo-optic coefficient to account for the change in refractive index, the optical resonance mode was then calculated based on the deformed shape (Fig.5b). The temperature was assumed to be uniform all across both the polymer and the pillar.

Upon observing the expansion resulting from a positive temperature change (Fig. 5c), it can be observed that the outer edge of the resonator expands outward by approximately

40 nm for a temperature increase of 10 °C, while also bending downward by around 20 nm for the same temperature change. This behavior is attributed to the difference in thermal expansion coefficients between the SU-8 material and the silicon substrate. Following the mode calculation, we extract both the effective refractive index and the change in the material's refractive index. They both exhibit a decrease with increasing temperature. Consequently, the resonance wavelength of the system will be influenced by both the change in refractive index and the geometric alterations resulting from the expansion.

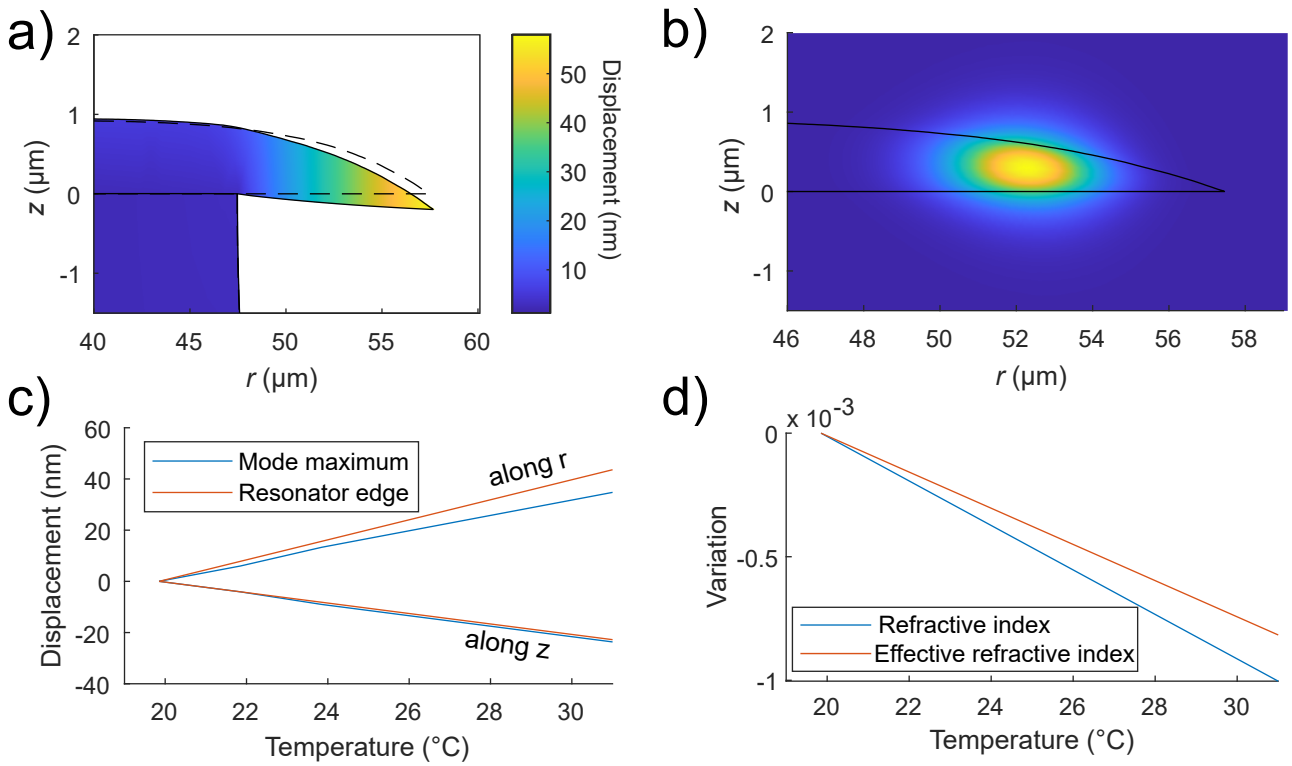

Figure 5: a) Simulated thermal expansion displacement field, with the displacement exaggerated by a factor of 5 for a temperature variation of 10 °C. b) Simulated optical mode, showcasing the electric field amplitude of the fundamental mode with the previous deformed resonator shape for a temperature variation of 10 °C. c) Displacement analysis of the mode maximum and drop edge along the r and z axes as temperature increases. d) Variation in refractive index change based on the thermo-optic coefficient and the effective refractive index with temperature.

In order to investigate the individual effects of the thermal expansion coefficient and the thermo-optic coefficient, simulations were conducted on the same device while setting

one coefficient to zero at a time. Figure 6a presents a comparison of the resonance wavelength shift with temperature for these separate cases. It is observed that the thermal expansion coefficient and the thermo-optic coefficient exhibit opposite effects. By carefully designing the device, these coefficients can counteract each other, resulting in a significantly reduced temperature sensitivity. However, when both effects are considered simultaneously, the combined contribution deviates from the simple summation of the effects obtained from individual simulations. This suggests that the two coefficients are not entirely linearly independent and may interact with each other in a more complex manner. For example, the expansion resulting from the thermal effects also impacts the effective refractive index of the system.

A previous study established a relationship between sensitivity to humidity for a rectangular disk[9] with a refractive index n, radius R, and undercut u. Drawing an analogy between humidity-related expansion $\left(\frac{\Delta\epsilon}{\Delta c}\right)$ and optical coefficients $\left(\frac{\Delta n}{\Delta c}\right)$ to thermal expansion $\left(\frac{\Delta\epsilon}{\Delta T}\right)$ and thermo-optic coefficients $\left(\frac{\Delta n}{\Delta T}\right)$, we can derive the thermal sensitivity (S) for the same disk as follows:

$$S = \lambda \left(\frac{\Delta\epsilon}{\Delta T} \frac{u}{R} + \frac{1}{n} \frac{\Delta n}{\Delta T} \right), \tag{1}$$

where λ represents the resonance wavelength. Notably, the thermal sensitivity exhibits a linear dependence with the ratio of the undercut to the radius (u/R). This relationship, however, may not hold true for drop-shape resonators due to their wedge profiles. Nevertheless, investigating the parameter u/R in our simulations provides valuable insights. Additionally, this relationship highlights the counteractive effects of the thermal expansion and thermo-optic coefficients. As the thermo-optic coefficient is negative, it is possible to choose an appropriate u/R value that cancels out both terms, resulting in a zero thermal sensitivity.

Such measurements were performed for various u/R ratios, and the wavelength shifts of different optical modes were tracked (Fig. 6b). It is observed that the sensitivity is more affected by the polarization than by mode numbers. Specifically, the transverse electric (TE)

modes consistently exhibit a red shift, causing their resonance peaks to shift towards longer wavelengths for all investigated u/R ratios. On the other hand, the transverse magnetic (TM) modes demonstrate zero sensitivity at an u/R ratio of approximately 30 %. Below this threshold, their resonance peaks undergo a blue shift, indicating a shift towards shorter wavelengths as the temperature increases. Throughout the remainder of the simulation study, the fundamental TM mode is selected for analysis. This mode exhibits the highest quality factor, making it the preferred choice for tracking and analyzing the corresponding resonance peak with the experimental data.

Figure 6c presents a comparison between the simulation results and the experimental study. The sensitivities of the six fabricated devices, each with a different undercut, are reported with a linear regression. The trend observed in the experimental data aligns closely with the simulation findings with a slightly different slope and a minor translation. The zero sensitivity point occurs around an u/R ratio of approximately 48 %. Several factors may contribute to the difference observed between the experimental and simulated results. These include potential errors in the measured thermal expansion and thermo-optic coefficients. Moreover, the microfabrication process itself can introduce variations in the polymer properties. Factors such as exposure to a vacuum chamber and plasma treatment during pillar etching can affect the mechanical properties of SU-8. Notably, the hardbake process of SU-8 has been identified as particularly influential in this regard[40,41]. Despite these potential variations, the simulation used the values provided in the datasheet for the material properties. Additionally, measurements of the resonator profile, undercut, and pillar shape inherently involve uncertainties, which can contribute to deviations in the observed sensitivities. Nevertheless, both the experimental and simulated data demonstrate positive slopes and pass through a point of zero temperature sensitivity, indicating the presence of a critical u/R ratio.

An empirical linear relationship between the thermal expansion and thermo-optic coefficients has been observed in polymers[42]. The coefficients obtained through ellipsometry

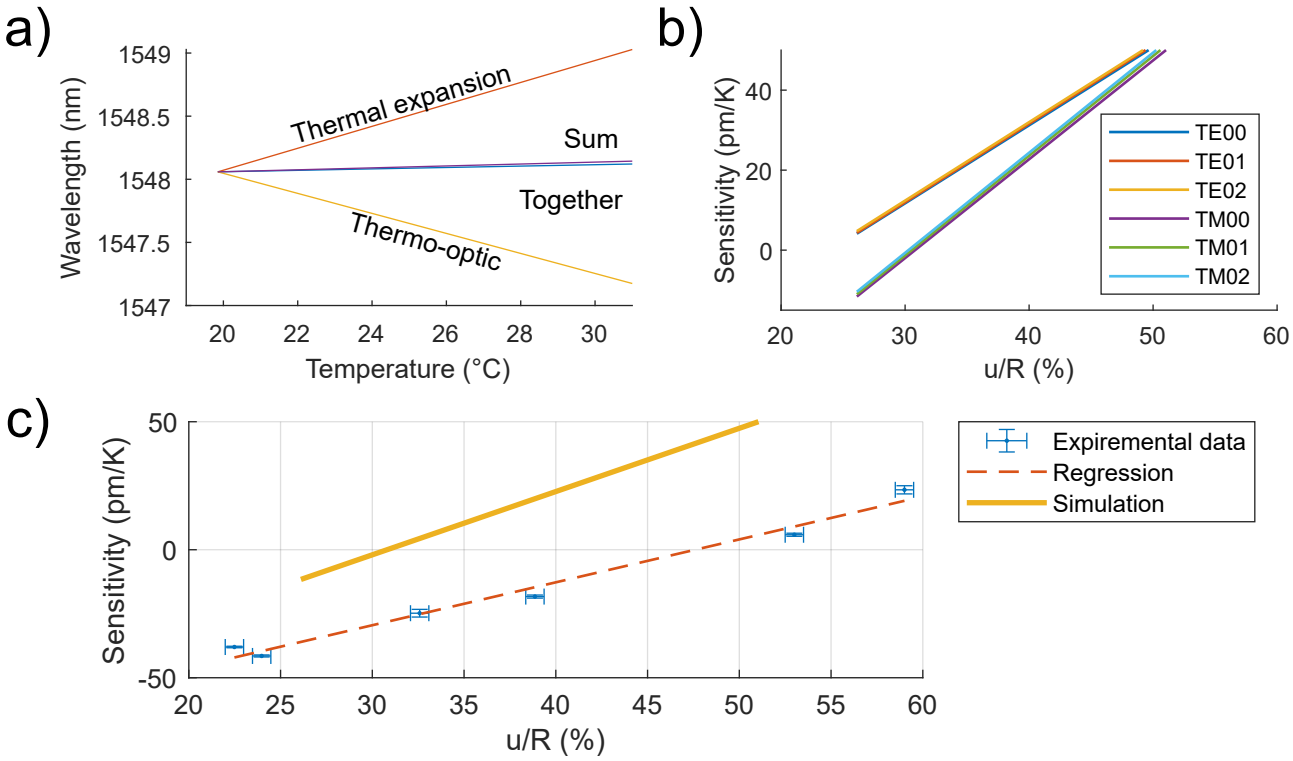

Figure 6: a) Study of the effect of both thermo-optic and thermal expansion coefficients on the resonance shift with temperature. b) Temperature sensitivity variation across u/R ratios for different modes of both TE and TM polarization. c) Comparative analysis between experimental results and simulation using measured coefficients.

measurements in this study closely align with this relationship. Specifically, for a thermal expansion coefficient of 150 ppm/K, the measured thermo-optic coefficient is −90 ppm/K, which deviates slightly from the expected value of −84 ppm/K. However, the thermo-optic coefficient value reported in the literature does not follow this trend when compared to the thermal expansion coefficient provided in the datasheet, which should be −29 ppm/K instead of −180 ppm/K.

The undercut parameter plays a crucial role in engineering the thermal sensitivity of a polymer resonator on pillar. Due to the complex geometry of the structure, determining the optimal undercut value for achieving minimal temperature sensitivity through simulation alone becomes challenging. Furthermore, the polymer properties are influenced by the intricacies of the fabrication process, making it difficult to precisely extract the properties of a microdroplet deposited by inkjet. Therefore, employing an empirical characterization approach to study the thermal sensitivity of devices with varying the u/R ratio proves to be an effective method for identifying an undercut value that exhibits insensitivity to temperature. This approach significantly reduces the impact of thermal noise crosstalk and enhances the overall performance of the sensor.

This study focus on a resonator with a drop shape to explore the possibility to use inkjet printing to fabricate an optical sensor made of polymer. Previous work with a polymer disk made with photolithography[9] did explore the temperature sensitivity for a unique u/R ratio of 16.7 % with a radius of 60 µm. The measured temperature sensitivity is reported to be −169.7 pm/°C which is much higher than what was reported for this study. It is closer to the simulation done with the literature values for the thermal expansion and thermo-optic coefficients. It is believed that the shape of the resonator impact the temperature sensitivity.

Although theoretically feasible to achieve complete temperature insensitivity with the suspended SU-8 resonator, uncertainties within the microfabrication process impose constraints on attaining the lowest possible temperature sensitivity. Experimentally, we managed to achieve a minimum temperature sensitivity of only 5.9 pm/°C, representing over 28 times

less sensitivity than the rectangular suspended SU-8 resonator[9]. In comparison, an SU-8 microcavity produced via inkjet printing and coated in PDMS[35] displays a temperature sensitivity of $-120\,\mathrm{pm/°C}$. For the latter case, given its attachment to the substrate, only the thermo-optic coefficient contributes to the sensitivity. In contrast to other polymer-based optical temperature sensors, our less sensitive resonator demonstrates sensitivity three orders of magnitude lower[43]. For instance, a silk fibroin microtoroid[44] showcases a temperature sensitivity of $1.17\,\mathrm{nm/°C}$.

Another approach previously reported to reduce the temperature sensitivity of a polymer-based optical resonator involves polymer annealing[25], resulting in a decrease of one order of magnitude (from $0.793\,\mathrm{nm/°C}$ to $0.068\,\mathrm{nm/°C}$). Through meticulous adjustment of design parameters, our approach achieves a comparable reduction in magnitude. Continued improvements in our technique hold the promise of achieving an even lower temperature sensitivity by enhancing control over the fabrication process.

Through the manipulation of the u/R ratio, precise control over the temperature sensitivity of the inkjet-printed optical resonator on pillar was achieved. This parameter allowed an insensitive sensor to temperature to be fabricated, as evidenced by the crossing of the temperature sensitivity through zero. By effectively mitigating the crosstalk between temperature fluctuations and the desired measured stimulus, the limitations imposed by the inherent temperature sensitivity of polymers were addressed. This ability to restrict and modulate temperature sensitivity is of great significance in the design of highly accurate and precise sensors.

5 Conclusion

The design approach employed in this study offers a convenient means of adjusting the temperature sensitivity of an optical resonator on pillar fabricated by combining inkjet printing technology and microfabrication. By adjusting the undercut, it becomes possible to achieve

extremely low sensitivity to temperature fluctuations. Such insensitivity to temperature minimizes crosstalk and enhances the sensor's precision in detecting other stimuli.

While this study primarily focused on investigating the influence of the u/R ratio on temperature sensitivity, other parameters can also be varied. For instance, the shape of the inkjet-printed droplet can impact the position of the resonant optical mode and, consequently, the effective refractive index. It is hypothesized that altering the shape, either by adjusting surface tension or by modifying the substrate and ink temperature during inkjet deposition, can affect the temperature sensitivity. Further research is required to explore these possibilities in more detail.

The u/R ratio is hypothesized to influence the sensitivity to various stimuli. This parameter, in conjunction with others, establishes a design space that necessitates exploration for effectively modulating the sensitivity to each stimulus. In cases where both the change in refractive index and thermal expansion exhibit an impact on sensitivity in the same trend, adjusting the u/R ratio can potentially enhance the sensitivity to that specific stimulus. A greater undercut allows for a larger region of the disk to undergo unconstrained expansion.

Finally, we have effectively addressed two key concerns associated with the polymeric whispering gallery mode resonator gas sensor. Employing drop-on-demand inkjet printing proved successful in fabricating the device, paving the way for the application of this fabrication technique to other polymers within the same microchip. Additionally, we propose a strategy to mitigate temperature cross-sensitivity through the optimization of a design parameter. This study systematically examines the dependence of temperature sensitivity on the u/R ratio, utilizing both experimental techniques and numerical simulations. By mitigating temperature sensitivity, we enhance the precision and expand the detection limits of our gas sensor.

This work represents an initial step towards a new sensing platform that combines polymer science with high-quality-factor optical resonators. The utilization of inkjet printing as an additive fabrication technique enables the integration of multiple polymers on a single

chip, offering the potential for developing multiplex sensors. To fully realize this goal, further investigations into different polymer materials and the integration of resonators through coupling to optical waveguides are necessary. It is believed that this platform holds significant promise for various sensing applications, such as gas sensing.

Acknowledgement

The author thanks the Microfabrication Laboratory (LMF) for the help with the microfabrication process, Rodrigo Itzamna Becerra Deana and Mikaël Leduc from the Fiber Optics Laboratory for the help in the fabrication of tapered optical fibers, Oleg Zabeida and Bill Baloukas from the Functional Coating and Surface Engineering Laboratory for the thermal expansion and thermo-optic coefficient measurement by ellipsometry and Prof. Richard Martel for the access to the drop-on-demand inkjet printer. This work was supported in part by the Fonds de recherche du Québec - Nature et technologies (FRQNT), (B2X 271283), the Natural Sciences and Engineering Research Council of Canada (NSERC), [RGPIN-2020-06692, ALLRP 577113-2022, ESD3-534843-2019] and the Canadian Microelectronics Corporation (CMC).

References

(1) Hu, L.; Zhang, Q.; Li, X.; Serpe, M. J. Stimuli-Responsive Polymers for Sensing and Actuation. *Materials Horizons* **2019**, *6*, 1774–1793.

(2) Dai, J.; Ogbeide, O.; Macadam, N.; Sun, Q.; Yu, W.; Li, Y.; Su, B.-L.; Hasan, T.; Huang, X.; Huang, W. Printed Gas Sensors. *Chemical Society Reviews* **2020**, *49*, 1756–1789.

(3) Zhao, H.; Bai, J. Highly Sensitive Piezo-Resistive Graphite Nanoplatelet–Carbon Nan-

otube Hybrids/Polydimethylsilicone Composites with Improved Conductive Network Construction. *ACS Applied Materials & Interfaces* **2015**, *7*, 9652–9659.

(4) Arshak, K. I.; McDonagh, D.; Durcan, M. A. Development of New Capacitive Strain Sensors Based on Thick Film Polymer and Cermet Technologies. *Sensors and Actuators A: Physical* **2000**, *79*, 102–114.

(5) Jiang, L.; Wu, J.; Chen, K.; Zheng, Y.; Deng, G.; Zhang, X.; Li, Z.; Chiang, K. S. Polymer Waveguide Mach-Zehnder Interferometer Coated With Dipolar Polycarbonate for On-Chip Nitroaromatics Detection. *Sensors and Actuators B: Chemical* **2020**, *305*, 127406.

(6) Heylman, K. D.; Knapper, K. A.; Horak, E. H.; Rea, M. T.; Vanga, S. K.; Goldsmith, R. H. Optical Microresonators for Sensing and Transduction: A Materials Perspective. *Advanced Materials* **2017**, *29*, 1700037.

(7) Zhu, N.; Shi, B.; Guo, Y.; Han, B.; nan Zhang, Y. Polydimethylsiloxane Self-Assembled Whispering Gallery Mode Microbottle Resonator for Ethanol Sensing. *Optical Materials* **2020**, *107*, 110024.

(8) Ji, P.; Zhu, M.; Liao, C.; Zhao, C.; Yang, K.; Xiong, C.; Han, J.; Li, C.; Zhang, L.; Liu, Y.; Wang, Y. In-Fiber Polymer Microdisk Resonator and Its Sensing Applications of Temperature and Humidity. *ACS Applied Materials & Interfaces* **2021**, *13*, 48119–48126.

(9) Lemieux-Leduc, C.; Guertin, R.; Bianki, M.-A.; Peter, Y.-A. All-Polymer Whispering Gallery Mode Resonators for Gas Sensing. *Optics Express* **2021**, *29*, 8685.

(10) Guertin, R.; Bianki, M.-A.; Lemieux-Leduc, C.; Peter, Y.-A. Multi-Gas Detection Using Fabry-Perot Interferometers on Silicon Chip. *Sensors and Actuators B: Chemical* **2021**, *335*, 129655.

(11) Yoshioka, H.; Ota, T.; Chen, C.; Ryu, S.; Yasui, K.; Oki, Y. Extreme Ultra-Low Lasing Threshold of Full-Polymeric Fundamental Microdisk Printed With Room-Temperature Atmospheric Ink-Jet Technique. *Scientific Reports* **2015**, *5*.

(12) Nasir, A.; Yatabe, R.; Mikami, Y.; Yoshioka, H.; Vasa, N.; Oki, Y. Ink-Jet Printed, Blended Polymer-Based Microdisk Resonators for Controlling Non-Specific Adsorption of Biomolecules. *Optics Letters* **2021**, *46*, 262–265.

(13) Tang, Z.; Fang, K.; Song, Y.; Sun, F. Jetting Performance of Polyethylene Glycol and Reactive Dye Solutions. *Polymers* **2019**, *11*, 739.

(14) Mikkonen, R.; Puistola, P.; Jönkkäri, I.; Mäntysalo, M. Inkjet Printable Polydimethylsiloxane for All-Inkjet-Printed Multilayered Soft Electrical Applications. *ACS Applied Materials & Interfaces* **2020**, *12*, 11990–11997.

(15) Šuly, P.; Krčmár, P.; Mašlík, J.; Urbánek, P.; Kuritka, I. Poly(vinyl Alcohol): Formulation of a Polymer Ink for the Patterning of Substrates With a Drop-On-Demand Inkjet Printer. *Materiali in tehnologije* **2017**, *51*, 41–48.

(16) Kiaee, M. M.; Maeder, T.; Brugger, J. Film Morphology Effect on Voc Sensor Performance Fabricated by Drop-On-Demand Inkjet-Printing. Proc. Actuators and Microsystems Eurosensors XXXIII (TRANSDUCERS EUROSENSORS XXXIII) 2019 20th Int. Conf. Solid-State Sensors. 2019; pp 1361–1364.

(17) Cichosz, S.; Masek, A.; Zaborski, M. Polymer-based Sensors: A Review. *Polymer Testing* **2018**, *67*, 342–348.

(18) Wang, S.; Yang, Y.; Niu, P.; Wu, S.; Liu, S.; Jin, R.-B.; Lu, P.; Hu, X.; Dai, N. Fiber Tip Michelson Interferometer for Temperature Sensing Based on Polymer-Filled Suspended Core Fiber. *Optics & Laser Technology* **2021**, *141*, 107147.

(19) Saha, N.; Brunetti, G.; Armenise, M. N.; Ciminelli, C. A Compact, Highly Sensitive pH Sensor Based on Polymer Waveguide Bragg Grating. *IEEE Photonics Journal* **2023**, *15*, 1–7.

(20) Ou, X.; Tang, B.; Zhang, P.; Li, B.; Sun, F.; Liu, R.; Huang, K.; Xie, L.; Li, Z.; Yang, Y. Microring Resonator Based on Polarization Multiplexing for Simultaneous Sensing of Refractive Index and Temperature on Silicon Platform. *Optics Express* **2022**, *30*, 25627.

(21) Chen, Y.; Zheng, Y.; Liang, D.; Zhang, Y.; Guo, J.; Lian, S.; Yu, Y.; Du, C.; Ruan, S. Fiber-Tip Fabry–Perot Cavity Pressure Sensor with UV-Curable Polymer Film Based on Suspension Curing Method. *IEEE Sensors Journal* **2022**, *22*, 6651–6660.

(22) Tong, R.; Wang, Y.; Zhao, K.-j.; Li, X.; Zhao, Y. Surface Plasmon Resonance Optical Fiber Sensor for Relative Humidity Detection Without Temperature Crosstalk. *Optics & Laser Technology* **2022**, *150*, 107951.

(23) Hu, J.; Chen, Y.; Ma, Z.; Zeng, L.; Zhou, D.; Peng, Z.; Sun, W.; Liu, Y. Temperature-Compensated Optical Fiber Sensor for Volatile Organic Compound Gas Detection Based on Cholesteric Liquid Crystal. *Optics Letters* **2021**, *46*, 3324.

(24) Han, S.; Alvi, N. U. H.; Granlöf, L.; Granberg, H.; Berggren, M.; Fabiano, S.; Crispin, X. A Multiparameter Pressure–Temperature–Humidity Sensor Based on Mixed Ionic–Electronic Cellulose Aerogels. *Advanced Science* **2019**, *6*, 1802128.

(25) Li, H.-C.; Wang, M.-Y.; Liu, B.; Liu, J.; Wang, Q.; He, X.-D.; Ping Chan, H.; Wang, D.; Yuan, J.; Wu, Q. Temperature-Independent Relative Humidity Sensing Properties of Polymer Micro-Bottle Resonators Coated with Graphene Oxide. *Measurement* **2022**, *196*, 111199.

(26) Han, M.; Wang, A. Temperature Compensation of Optical Microresonators Using a Surface Layer With Negative Thermo-Optic Coefficient. *Optics Letters* **2007**, *32*, 1800.

(27) Fakhfouri, V.; Cantale, N.; Mermoud, G.; Kim, J.; Boiko, D.; Charbon, E.; Martinoli, A.; Brugger, J. Inkjet Printing of SU-8 for Polymer-Based MEMS a Case Study for Microlenses. 2008 IEEE 21st International Conference on Micro Electro Mechanical Systems. 2008.

(28) Voigt, A.; Ostrzinski, U.; Pfeiffer, K.; Kim, J. Y.; Fakhfouri, V.; Brugger, J.; Gruetzner, G. New Inks for the Direct Drop-On-Demand Fabrication of Polymer Lenses. *Microelectronic Engineering* **2011**, *88*, 2174–2179.

(29) Jacot-Descombes, L.; Gullo, M. R.; Mastrangeli, M.; Cadarso, V. J.; Brugger, J. Inkjet Printed SU-8 Hemispherical Microcapsules and Silicon Chip Embedding. *Micro & Nano Letters* **2013**, *8*, 633–636.

(30) Bernasconi, R.; Angeli, M. C.; Mantica, F.; Carniani, D.; Magagnin, L. SU-8 Inkjet Patterning for Microfabrication. *Polymer* **2019**, *185*, 121933.

(31) Eryürek, M.; Tasdemir, Z.; Karadag, Y.; Anand, S.; Kilinc, N.; Alaca, B.; Kiraz, A. Integrated Humidity Sensor Based on SU-8 Polymer Microdisk Microresonator. *Sensors and Actuators B: Chemical* **2017**, *242*, 1115–1120.

(32) Du, Z.; Yu, X.; Han, Y. Inkjet Printing of Viscoelastic Polymer Inks. *Chinese Chemical Letters* **2018**, *29*, 399–404.

(33) Soltman, D.; Subramanian, V. Inkjet-Printed Line Morphologies and Temperature Control of the Coffee Ring Effect. *Langmuir* **2008**, *24*, 2224–2231.

(34) Chen, C.; Wan, L.; Chandrahalim, H.; Zhou, J.; Zhang, H.; Cho, S.; Mei, T.; Yoshioka, H.; Tian, H.; Nishimura, N.; Fan, X.; Guo, L. J.; Oki, Y. Effects of Edge Inclination Angles on Whispering-Gallery Modes in Printable Wedge Microdisk Lasers. *Optics Express* **2018**, *26*, 233.

(35) Zhang, Z.; Yao, N.; Pan, J.; Zhang, L.; Fang, W.; Tong, L. A New Route for Fabricating Polymer Optical Microcavities. *Nanoscale* **2019**, *11*, 5203–5208.

(36) Su-8 2000 Permanent Epoxy Negative Photoresist. version 4, MicroChem.

(37) Xie, N.; Hashimoto, T.; Utaka, K. Very Low Power Operation of Compact MMI Polymer Thermooptic Switch. *IEEE Photonics Technology Letters* **2009**, *21*, 1335–1337.

(38) Yan, Y.-F.; Zheng, C.-T.; Liang, L.; Meng, J.; Sun, X.-Q.; Wang, F.; Zhang, D.-M. Response-Time Improvement of A 2×2 Thermo-Optic Switch With Polymer/silica Hybrid Waveguide. *Optics Communications* **2012**, *285*, 3758–3762.

(39) Liu, Y.-F.; Wang, X.-B.; Sun, J.; Gu, H.-J.; Sun, X.-Q.; Chen, C.-M.; Wang, F.; Zhang, D.-M. Thermal Field Analysis of Polymer/silica Hybrid Waveguide Thermo-Optic Switch. *Optics Communications* **2015**, *356*, 79–83.

(40) Feng, R.; Farris, R. J. Influence of Processing Conditions on the Thermal and Mechanical Properties of SU8 Negative Photoresist Coatings. *Journal of Micromechanics and Microengineering* **2002**, *13*, 80–88.

(41) Gunde, M. K.; Hauptman, N.; Maček, M.; Kunaver, M. The Influence of Hard-Baking Temperature Applied for SU8 Sensor Layer on the Sensitivity of Capacitive Chemical Sensor. *Applied Physics A* **2008**, *95*, 673–680.

(42) Zhang, Z.; Zhao, P.; Lin, P.; Sun, F. Thermo-Optic Coefficients of Polymers for Optical Waveguide Applications. *Polymer* **2006**, *47*, 4893–4896.

(43) Szczerska, M. Temperature Sensors Based on Polymer Fiber Optic Interferometer. *Chemosensors* **2022**, *10*, 228.

(44) Xu, L.; Jiang, X.; Zhao, G.; Ma, D.; Tao, H.; Liu, Z.; Omenetto, F. G.; Yang, L. High-Q Silk Fibroin Whispering Gallery Microresonator. *Optics Express* **2016**, *24*, 20825.

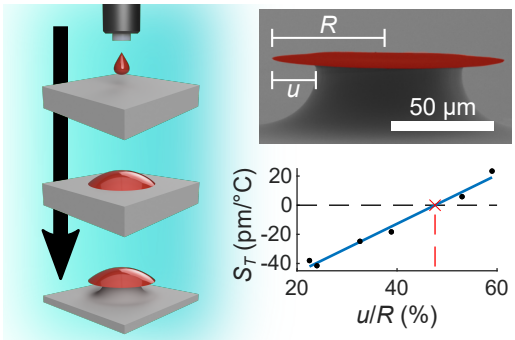

Figure 7: For Table of Contents Only